University of Groningen

A series of 1-D zinc(II) coordination polymers with 3-D supramolecular networks

Zahedi, Mansoureh; Shaabani, Behrouz; Radyousefnia, Negar; Englert, Ulli; Blake, Graeme R.; Aygun, Muhittin

IMPORTANT NOTE: You are advised to consult the publisher's version (publisher's PDF) if you wish to cite from it. Please check the document version below.

Document Version
Publisher's PDF, also known as Version of record

Publication date:
2018

[Link to publication in University of Groningen/UMCG research database](#)
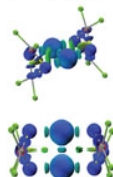
A series of 1-D zinc(II) coordination polymers with 3-D supramolecular networks: synthesis, structural investigation, and NBO analysis

Mansoureh Zahedi, Behrouz Shaabani, Negar Radyousefnia, Ulli Englert, Graeme R. Blake & Muhittin Aygün

View supplementary material

Accepted author version posted online: 21 Nov 2018.
Published online: 24 Jan 2019.

Submit your article to this journal

Article views: 58

View Crossmark data

Taylor & Francis
Taylor & Francis Group

Check for updates

A series of 1-D zinc(II) coordination polymers with 3-D supramolecular networks: synthesis, structural investigation, and NBO analysis

Mansoureh Zahedi[a], Behrouz Shaabani[a], Negar Radyousefnia[a], Ulli Englert[b] (iD), Graeme R. Blake[c] and Muhittin Aygün[d]

[a]Department of Inorganic Chemistry, Faculty of Chemistry, University of Tabriz, Tabriz, Iran; [b]Institute of Inorganic Chemistry, RWTH Aachen University, Aachen, Germany; [c]Zernike Institute for Advanced Materials, University of Groningen, Groningen, The Netherlands; [d]Department of Physics, Faculty of Arts & Sciences, Dokuz Eylul University, Izmir, Turkey

ABSTRACT

N,N′-Bis(pyridin-4-ylmethylene)naphthalene-1,5-diamine (L) acts as a bipyridine analogue linker ligand towards $\{Zn_7(\mu_4\text{-O})_2(OAc)_{10}\}$, $\{Zn_2(NCS)_2(OAc)_2\}$, and $\{Zn(N_3)_2\}$ nodes and allows construction of three new 1-D coordination polymers, the linear chain $[Zn_7(\mu_4\text{-O})_2(OAc)_{10}(L)]_n$ (**1**), $[Zn(NCS)(OAc)(L)]_n$ (**2**) in ladder-type geometry and the zigzag chain $[Zn(N_3)_2(L)]_n$ (**3**). Structural characterization reveals that in **1** acetate anionic ligands connect seven Zn(II) ions through the bridging coordination modes $\mu_3\text{-}\eta^1,\eta^2$ and $\mu_2\text{-}\eta^1,\eta^1$. The resulting heptanuclear node is located on an inversion center and therefore consists of four crystallographically distinct cations; their coordination spheres correspond to distorted octahedra or tetrahedra. The Zn(II) ions in polymer **2** exhibit distorted trigonal bipyramidal $\{ZnN_3O_2\}$ coordination; $\mu_2\text{-}\eta^1,\eta^1$ coordinated acetate and terminal thiocyanate ligands lead to inversion-symmetric $[Zn_2(NCS)_2(OAc)_2]$ secondary building units (SBU), which are further linked by the *N,N′*-bipyridine analogue L. Terminal coordination of two anionic azide ligands and the bridging bipyridine L result in coordination polymer **3**, in which the cations adopt distorted tetrahedral $\{ZnN_4\}$ coordination. In all crystalline solids **1–3**, adjacent 1-D chains interact through $\pi-\pi$ stacking and non-classical $(C-H\cdots O, C-H\cdots\pi)$ hydrogen bonds, leading to 3-D supramolecular architectures. Differences in their 3-D arrangement are due to variations in the anionic co-ligands, subtle conformational differences in the semi-rigid linker and the variable coordination sphere about the zinc cations. Thermogravimetric investigations indicate differences in both thermal stability and decomposition mode. Natural bond orbital (NBO) analysis provides a convenient basis for investigating the intramolecular bonding interactions and delocalization effects in these molecular systems. Finally, solids **1–3** exhibit intense luminescence at room temperature.
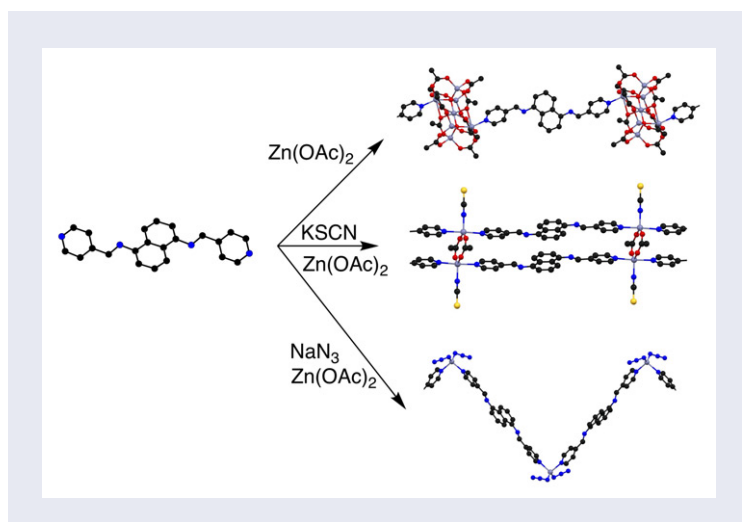
1. Introduction

Over the past few decades, the development of new coordination polymers (CPs) and metal–organic frameworks (MOFs), involving their synthesis and characterization as well as the study of their structural and physical properties, has attracted much attention owing to their large variety of topologies and potential applications [1–6]. The metal nodes and their coordination geometry, the multidentate spacer ligands, the selection of counter anions in the case of cationic networks and supramolecular interactions such as hydrogen bonding or π–π stacking have emerged as key factors responsible for the overall structure of these materials.

In particular, the organic linker ligands with their specific structural features and functional groups can dramatically influence both the topology and composition of the resulting coordination polymers. In this context, 4,4′-bipyridine analogue ligands are important multidentate N,N'-donor ligands because of their excellent coordination ability and distinctive structural properties. In combination with metal cations, the variable intraligand geometry, the versatility in the spacer part and the influence on the packing process through intermolecular π–π interactions have led to networks with unusual structures and prominent architectures [7–9]. N,N'-Bis(pyridin-4-ylmethylene)-naphthalene-1,5-diamine represents an attractive spacer for the synthesis of coordination polymers. Su et al. first made use of this linker ligand in the synthesis of a 1-D ladder-shaped coordination polymer $[Co_2L_3(NO_3)_4]_n$ and a 3-D network $[Cd_2L_3(NO_3)_4]_n$ [10]. Min et al. devoted an extensive study to this linker and were able to design and prepare a series of coordination polymers derived of L [11–13]. Li et al. introduced 1-D and 2-D structures in which L is coordinated to Fe(II) cations [14]. Previous systematic work from our group on the synthesis of coordination polymers containing this dipyridyl ligand is documented [15–17].

The incorporation of anions plays a decisive role when neutral bridging ligands are combined with cationic nodes [18, 19]. A counter-anion with variable coordination

Zn(OAC)$_2$·2H$_2$O
MeOH, EtOH/ THF

[Zn$_7$(μ$_4$-O)$_2$(OAc)$_{10}$(L)]$_n$ (1)

1-D chain structure

KSCN/Zn(OAc)$_2$·2H$_2$O
MeOH/ DCM

[Zn(SCN)(OAc)(L)]$_n$ (2)

1-D ladder-like structure

NaN$_3$/ Zn(OAc)$_2$·2H$_2$O
MeOH

[Zn(N$_3$)$_2$(L)]$_n$ (3)

1-D zigzag structure
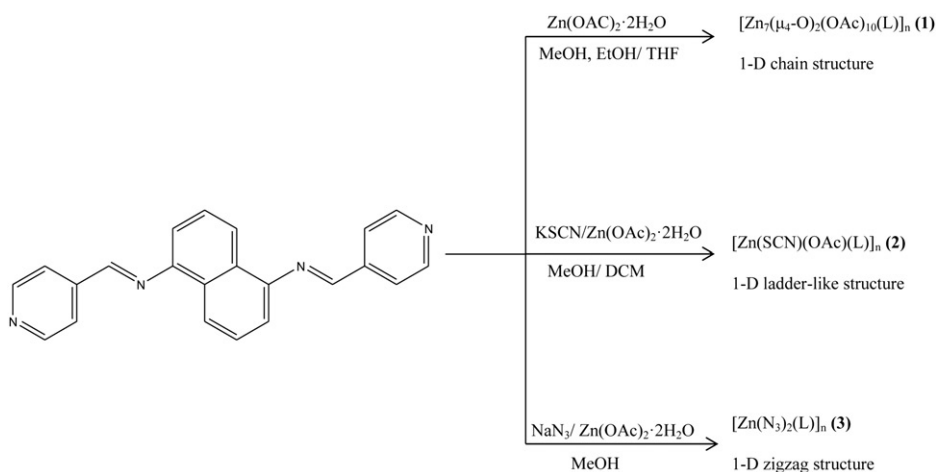
Scheme 1. Summary of the coordination polymers synthesized and structurally characterized.

ability, including various bridging or terminal modes, may act as nucleophile and compete with the organic spacer ligands for metal coordination. It can thus control the coordination number of the cation and the dimensionality of the resulting extended structures [20, 21]. Moreover, the steric requirements of a terminally coordinated anion have crucial influence on the structure; a small anion may lead to an interpenetrated network, whereas an elongated and sterically more demanding anion can prevent interpenetration and result in a simple stacking of adjacent layers [22].

In this contribution we use L and tune the anionic co-ligand (acetate, thiocyanate, and azide) to obtain the three new 1-D coordination polymers shown in Scheme 1, [Zn$_7$(μ$_4$-O)$_2$(OAc)$_{10}$(L)]$_n$ (**1**), [Zn(NCS)(OAc)(L)]$_n$ (**2**), and [Zn(N$_3$)$_2$(L)]$_n$ (**3**). Complexes **1–3** have been characterized by infrared spectroscopy (FT-IR), elemental and thermal analysis, and luminescence spectroscopy. Single crystal X-ray diffraction has allowed us to deduce their structure at atomic resolution, and powder diffraction ensured phase purity of the solids. The anionic co-ligands represent a tool to modify structural aspects in the coordination polymers such as the stereochemistry at the cations and the dimensionality of the extended structures, and we address the effect of intermolecular interactions in the expansion of the material perpendicular to the direction of the polymer chain. Finally, natural bond orbital analysis (NBO) using the DFT method and solid state electronic properties have been investigated for our target coordination polymers.

2. Experimental

2.1. Materials and physical measurements

All reagents and solvents were commercially available and used without purification. L was prepared according to the literature [15]. Elemental analyses were performed using a Heraeus CHNO-Rapid VarioEL. FT-IR spectra were measured using a Nicolet Avatar 360 E.S.P. spectrometer and a Bruker Tensor 27. TG and SDTA analyses were performed in air with a heating rate of 5 K min^{-1} from 25–800 °C on a Mettler Toledo

TGA/SDTA 851e instrument. X-ray powder diffraction patterns were obtained at ambient temperature on flat samples with a Stoe Imageplate Detector IP-PSD operating with Cu-Kα1 radiation. Fluorescence and UV–Vis spectra were measured using Perkin Elmer LS45 and Phystec UV–Vis miniaturism PL-2500, respectively.

2.2. Preparation of coordination polymers

2.2.1. Deca(acetato)-di(μ₄-oxo)-(N,N′-bis(pyridin-4-ylmethylene)naphthalene-1,5-diamine)-hepta-zinc(II), [Zn₇(μ₄-O)₂(OAc)₁₀(L)]ₙ (1)

An ethanol solution (6 mL) of $Zn(OAc)_2 \cdot 2H_2O$ (21.90 mg, 0.1 mmol) was added to a solution of L (33.60 mg, 0.1 mmol) in acetonitrile (6 mL). The mixture was stirred and refluxed for 3 h. The yellow precipitate was recovered by filtration and washed with ethanol. Yield: 41%, 58 mg. Yellow block-shaped single crystals were obtained by slow reactant diffusion. $Zn(OAc)_2 \cdot 2H_2O$ (10.97 mg, 0.05 mmol) was dissolved in a mixture of methanol and ethanol (1:5, 6 mL) and carefully layered on top of a solution of L (16.80 mg, 0.05 mmol) in tetrahydrofuran (6 mL). IR (KBr, cm^{-1}): 3060(w), 2990(w), 2869(w), 1633(vs), 1617(m), 1428(vs), 1322(w), 1228 (w), 1030(w), 925(w) 834 (w), 794 (m), 665(m). Crystals were formed after 3 days. Freshly prepared crystals of **1** contain seven molecules of THF per formula unit; this co-crystallized solvent evaporates upon drying as also indicated by the powder pattern. Anal. Calcd for the solvent-free compound $C_{42}H_{46}N_4O_{22}Zn_7$: C, 35.61; H, 3.27; N, 3.96. Found: C, 35.37; H, 3.34; N, 4.19%.

2.2.2. Acetato-(N,N′-bis(pyridin-4-ylmethylene)naphthalene-1,5-diamine)-(thiocyanato)-zinc(II), [Zn(NCS)(OAc)(L)]ₙ (2)

Solutions of KSCN (4.85 mg, 0.05 mmol) in methanol (2 mL) and $Zn(OAc)_2 \cdot 2H_2O$ (10.97 mg, 0.05 mmol) in methanol (4 mL) were mixed and stirred for 15 min. This solution was carefully layered on top of a solution of L (16.80 mg, 0.05 mmol) in dichloromethane (4 mL). Orange block-shaped single crystals suitable for X-ray diffraction formed in the contact layer within 2 days. Yield: 48%, 12.45 mg. IR (KBr, cm^{-1}): 3070(w), 2923(w), 2849(w), 2070(s), 1608(s), 1593(vs), 1558(m), 1443(s), 1417(s), 1313(m), 1238(w), 1058(w), 1016(m), 972(m), 823(s), 781(s), 656(s), 539(m). Anal. Calcd for $C_{25}H_{19}N_5O_2SZn$: C, 57.87; H, 3.69; N, 13.50. Found: C, 58.09; H, 3.48; N, 13.37%.

2.2.3. Di(azido)-(N,N′-bis(pyridin-4-ylmethylene)naphthalene-1,5-diamine)-zinc(II) [Zn(N₃)₂(L)]ₙ (3)

Yellow crystals of **3** were obtained using the thermal gradient method in a branched tube [23]. L (672.0 mg, 2.0 mmol), $Zn(OAc)_2 \cdot 2H_2O$ (439.0 mg, 2.0 mmol) and sodium azide (8.0 mmol, 480.0 mg) were placed at the bottom of the main arm of a glass tube, which was then slowly filled with methanol. The tube was sealed and the arm containing the reactants was immersed in an oil bath at 60 °C while the other arm was kept at ambient temperature. Single crystals suitable for measurement formed after 3 days. Yield: 56%, 544.1 mg. IR (KBr, cm^{-1}): 2925(w), 2854(w), 2056(vs), 1614(s), 1460(w), 1420(m), 1323(m), 1283(w), 1125(w), 1026(w), 970(w), 860(w), 822(m), 651(w), 504(m). Anal. Calcd for $C_{22}H_{16}N_{10}Zn$: C, 54.39; H, 3.32; N, 28.83. Found: C, 54.18; H, 3.35; N, 29.06%.

Table 1. Crystal data and refinement results for **1–3**.

Compound	1	2	3
Chemical formula	$C_{70}H_{102}N_4O_{29}Zn_7$	$C_{25}H_{19}N_5O_2SZn$	$C_{22}H_{16}N_{10}Zn$
M_r	1921.14	518.88	485.82
Crystal system, space group	Triclinic, P-1	Triclinic, P-1	Orthorhombic, $Pbca$
a, b, c (Å)	10.0100(18), 11.549(2), 17.715 (3)	8.7231(8), 9.1757(8), 16.3264(14)	14.328(2), 11.0832(19), 26.635(4)
α, β, γ (°)	99.410(3), 104.887(3), 105.573(3)	75.710(3), 88.850(7), 65.336(9)	–
V (Å^3)	1846.1(6)	1145.70(17)	4229.5(11)
Z	1	2	8
μ (mm^{-1})	2.32	1.20	1.20
Crystal size (mm)	$0.31 \times 0.15 \times 0.15$	$0.29 \times 0.14 \times 0.10$	$0.40 \times 0.04 \times 0.04$
Absorption correction	Multi-scan	Analytical	Multi-scan
$(\sin \theta/\lambda)$max (Å^{-1})	0.722	0.625	0.558
R_{int}	0.115	0.054	0.099
R_1, wR_2, S	0.067, 0.122, 1.02	0.064, 0.141, 0.94	0.066, 0.186, 1.11
No. indep. reflections	9776	4669	3034
No. parameters	345	308	298
$\Delta\rho_{max}, \Delta\rho_{min}$ (e Å^{-3})	1.37, −1.95	0.87, −0.51	1.08, −0.81

2.3. X-ray data collection and structure determination

Crystal data and data collection parameters are compiled in Table 1. Intensity data for **1–3** were collected at 100 K on a Bruker D8 diffractometer equipped with an APEX CCD area detector (Mo-Kα radiation, $\lambda = 0.71073$ Å, Incoatec microsource with multi-layer optics) at 293 K on an Xcalibur four-circle diffractometer equipped with an EOS CCD detector (Mo-Kα radiation) and at 100 K on a Bruker D8 Venture diffractometer equipped with a Photon100 area detector (Mo-Kα radiation, focusing multilayer optics), respectively. Intensities for **1** and **3** were integrated with SAINT [24] and absorption corrections were made by multi-scan methods with SADABS [25]. The CrysAlisPro software [26] was used for data collection, cell refinement, and data reduction of **2**.

All structures were solved by direct methods (SHELXS-97) [27] and refined by full matrix least squares based on F^2 as implemented in SHELXL-97 [27] or SHELXL-2014 [28]. No disorder model with atomic resolution could be assigned to the co-crystallized tetrahydrofuran in **1**, and hence the PLATON SQUEEZE [29] procedure was used to account for the contribution of the disordered solvent to the calculated structure factors. One large solvent accessible volume per unit cell was associated with a volume of 686 Å^3 and contained 259 electrons, in good agreement with seven tetrahydrofuran solvent molecules. Nonhydrogen atoms were treated anisotropically. Hydrogens bonded to C were placed at geometrically calculated positions and refined using a riding model. Isotropic displacement parameters for all hydrogens were constrained to $U_{iso}(H) = 1.2U_{eq}(C)$.

2.4. Theoretical calculations

Natural atomic charges, electron configurations, second-order perturbation energies, and frontier molecular orbital energy levels were obtained by single point calculations through natural bond orbital (NBO) analysis. The molecular structure parameters and

starting atomic coordinates for the calculations were taken from the diffraction results. Density functional theory (DFT) calculations were performed with the GAUSSIAN03 program package [30] at hybrid functional B3LYP level [31]. The effective core potential basis set Lanl2dz [32] was applied for metal atoms, and a 6-31G* basis set [33] was used for all nonmetal atoms.

3. Results and discussion

3.1. Synthesis and preliminary characterization

Crystalline products were obtained from reactions of zinc acetate dihydrate $(Zn(OAc)_2 \cdot 2H_2O)$ with L in 1:1 stoichiometry for **1**, with potassium thiocyanate in the same molar ratio for **2** and with excess sodium azide for **3**. Slow reactant diffusion or thermal gradient methods afforded single crystals of 1-D coordination polymers; they are insoluble in conventional solvents such as THF, DMF, CHCl$_3$, and CCl$_4$.

The FT-IR spectra of the products exhibit strong absorption frequencies at wavenumbers of 1617 cm^{-1} (for **1**), 1608 cm^{-1} (for **2**) and 1614 cm^{-1} (for **3**), assigned to C=N bond stretching of the linker ligand, which smoothly shifted to lower wavenumbers on complexation. Furthermore, very strong bands are displayed for ν_{asy} (COO$^-$) [1633 cm^{-1} (**1**); 1593 cm^{-1} (**2**)] and ν_{sym} (COO$^-$) [1428 cm^{-1} (**1**); 1417 cm^{-1} (**2**)]. The differences in wavenumber between these bands, $\Delta\nu$ (ν_{asym}(COO$^-$) $-$ ν_{sym}(COO$^-$)), amount to 205 and 176 cm^{-1} for **1** and **2**. When compared to the same wavenumber difference for sodium acetate [34, 35] this $\Delta\nu$ indicates that the acetate ions are bonded to the zinc metal cation in a bridging mode, in agreement with the X-ray diffraction results. In the FT-IR spectrum of thiocyanato zinc complex **2**, a strong vibration at 2070 cm^{-1} can be attributed to the ν_{asym} stretching band in the NCS moiety. The absorption frequency below 2100 cm^{-1} proves coordination via the N atom and the terminal nature of the thiocyanato ligand [36, 37]. The characteristic asymmetric stretching vibration of the N$_3^-$ ligand in **3** is observed as a strong band at 2056 cm^{-1}, and the symmetric stretching mode is exhibited at 1346 cm^{-1} [37, 38]. Finally, several weak absorptions in the range 3060–2849 cm^{-1} can be assigned to aromatic, aliphatic, and iminic C–H stretching vibrations (IR spectra for L and **1**–**3** are included in the Supporting Information Figures S4–S7).

The CHN elemental analysis data are in accord with the calculated values (see Section 2.2) and confirm the results of our single crystal X-ray diffraction experiments for the bulk. The powder diffraction patterns of **2** and **3** correspond well with those simulated from the single crystal data. Minor differences between measured and simulated patterns are observed for **1**, indicating at least partial desolvation (Supporting Information Figures S1–S3).

3.2. Crystal structures

3.2.1. [Zn$_7$(μ$_4$-O)$_2$(OAc)$_{10}$(L)]$_n$ (1)

Single-crystal X-ray diffraction analysis revealed that coordination polymer **1** crystallizes in the triclinic space group $P\bar{1}$. This structure is based on a tightly bound {Zn$_7$(μ$_4$-O)$_2$(OAc)$_{10}$} node. Seven Zn(II) ions are connected through acetato ligands in bridging
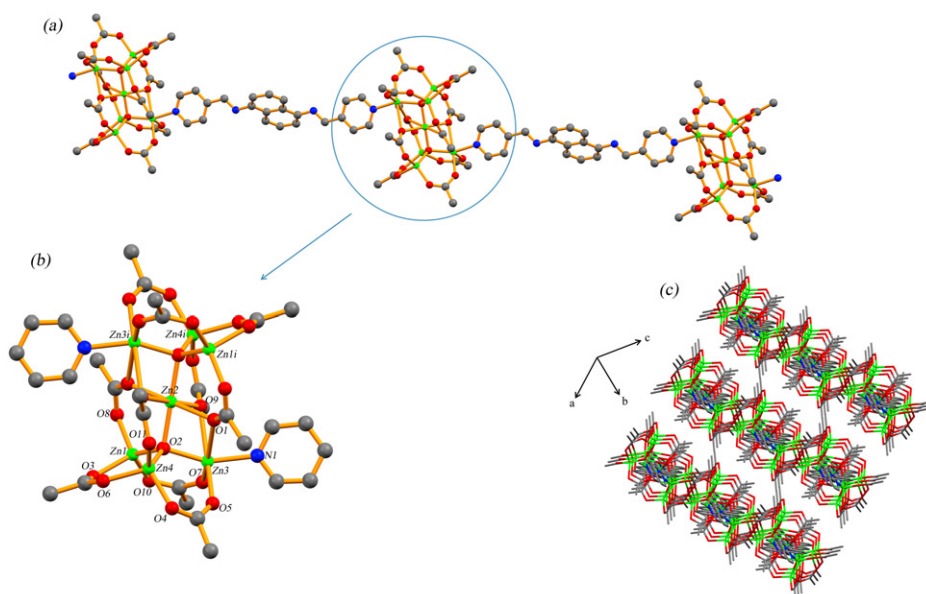
Figure 1. (a) 1-D linear chain structure **1**. (b) Heptanuclear center {Zn$_7$(μ_4-O)$_2$(OAc)$_{10}$}. Symmetry operators $i = -x+1, -y, -z$. (c) Packing in polymer direction along [1–11]. Hydrogens have been omitted for clarity.

coordination modes μ_3-η^1,η^2 and μ_2-η^1,η^1 and also through two oxo ligands. The corresponding heptanuclear units are connected by the bipyridine analogue linker L, resulting in a 1-D polymer (Figure 1(a)). Each heptanuclear core sits about a crystallographic center of inversion, with 3.5 cations in the asymmetric unit (Figure 1(b)). The Zn1 and Zn4 centers are best described as slightly distorted tetrahedra; their four-coordinate structural indices according to Yang *et al*. [39] amount to 0.91 and 0.90, respectively. The coordination sphere comprises three oxygen atoms from three different acetate groups and one oxygen atom of the oxo bridge. Zn2 is located at the center of this core and hence in the crystallographic inversion center; it has a distorted octahedral {ZnO$_6$} coordination environment in which the axial positions are occupied by the oxo bridges and the equatorial plane is occupied by four oxygen atoms from four different acetato ligands. Finally, Zn3 adopts a distorted octahedral geometry {ZnNO$_5$}, coordinated by one oxygen atom of an oxo bridge and four oxygen atoms of the acetate groups, which link this cation to the other Zn(II) in the heptanuclear nodes. A nitrogen atom from the bipyridine bridge completes the octahedral coordination about Zn3 and connects adjacent nodes to form a chain. This compound shares similarities with several structures published earlier [40–42], the linear coordination polymers [Zn$_7$(μ_4-O)$_2$(OAc)$_{10}$(3pdb)]$_n$ (3pdb = 1,4-*bis*(3-pyridyl)-2,3-diaza-1,3-butadiene) and [Zn$_7$(μ_4-O)$_2$(OAc)$_{10}$(4pdb)]$_n$ (4pdb = 1,4-*bis*(4-pyridyl)-2,3-diaza-1,3-butadiene) [41], as well as the discrete complex [Zn$_7$(μ_4-O)$_2$(OAc)$_{10}$(Pz)$_2$] (Pz = pyrazine) [42]. Details about the coordination geometry in **1** are available in the Supporting Information (Table S1).

Adjacent chains in **1** are arranged in an alternating mode through nonclassical C–H⋯O hydrogen bonds between L ligands and the acetate groups [H⋯O = 2.65 Å
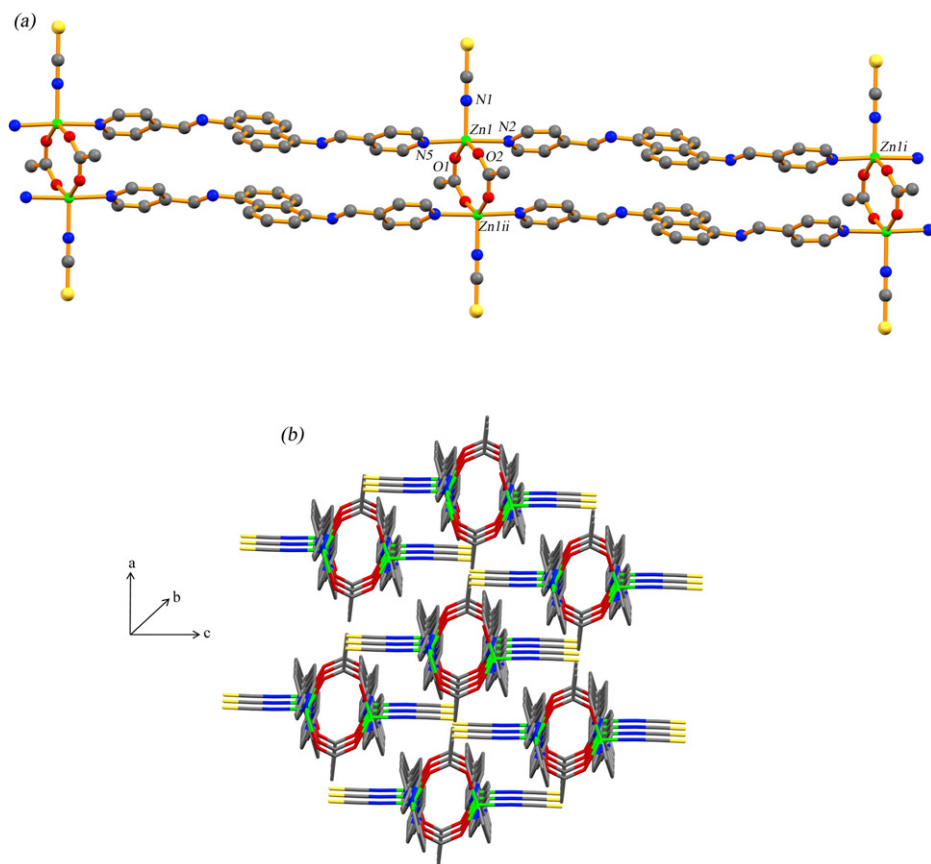
Figure 2. (a) 1-D ladder-like structure **2**. Symmetry operators $i = x - 1$, $y + 2$, $z - 1$; $ii = -x$, $2 - y$, $-z$; (b) Packing in polymer direction along [1–21]. Hydrogens have been omitted for clarity.

and 2.56 Å] and via interstrand C–H···π hydrogen bonds of 2.76 Å between the pyridine rings of the linker and the acetate groups of neighboring chains; these interactions stabilize an overall 3-D supramolecular polymeric structure (Figure 1(c)).

3.2.2. [Zn(NCS)(OAc)(L)]$_n$ (2)

Coordination polymer **2** crystallizes in the triclinic space group $P\bar{1}$. The asymmetric unit of this compound corresponds to the formula [Zn(NCS)(OAc)(L)]. The Zn(II) ion is located in the center of a distorted trigonal bipyramid, characterized by a τ_5 index of 0.68 according to Addison *et al.* [43]. The coordination sphere is defined by two oxygen atoms from two acetate groups, one nitrogen atom of the thiocyanato ligand and two nitrogen atoms from two bipyridine analogue linkers. The acetato co-ligands bridge two Zn cations in μ_2-η^1,η^1 fashion, whereas thiocyanate is *N*-coordinated as a terminal ligand to form a secondary building unit of {Zn$_2$(NCS)$_2$(OAc)$_2$} with a Zn···Zn distance of 3.69 Å. The *N,N′*-bipyridine analogue ligand links adjacent units to form a 1-D ladder-like coordination polymer (Figure 2(a)). A search in the CSD data base [44] indicates that the extended compounds [Zn(C$_{12}$H$_8$N$_2$)]$_2$[C$_{12}$N$_2$H$_8$(COO)$_2$]$_2$·(C$_6$H$_{12}$O)·(H$_2$O)
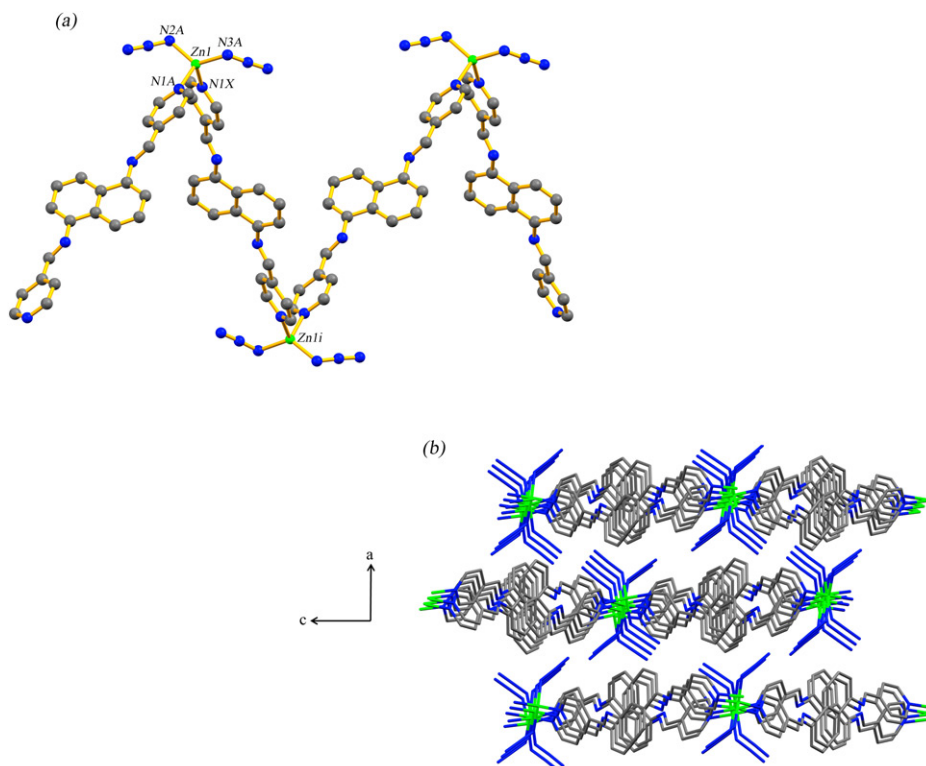
Figure 3. (a) 1-D zigzag structure **3**. Symmetry operators $i = x$, $1.5 - y$, $0.5 + z$. (b) Packing in polymer direction along [1-1-1]. Hydrogens have been omitted for clarity.

[45] and [Zn(bpe)(OH-BDC)]$_n$ (OH-H$_2$BDC = 5-hydroxyisophthalic acid, bpe = 1,2-*bis*(4-pyridyl)ethane) [46] are among the limited number of structures that exhibit Zn(II) in trigonal-bipyramidal geometry and coordinated to 4,4'-bipyridyl analogue derivatives. Our previously reported 1-D coordination polymer {[ZnL(OAc)$_2$]·C$_2$H$_5$OH}$_n$ (L = *N,N'*-(3,3'-dimethyl-4,4'-biphenyldiyl)*bis*[1-(3-pyridinyl)methanimine) displays a topology comparable to this new structure [21]; it exhibits similarities in connectivity, the coordination mode of the bridging acetato co-ligand, and in the metal ion coordination geometry. The Zn − N and Zn − O bond lengths (Supporting Information Table S2) are close to the corresponding values in the related structures.

Perpendicular to the polymer strand, the individual chains are further connected through π–π stacking (closest C···C distances of 3.39 and 3.61 Å) and C − H···π hydrogen bonds (2.76 Å) between the aromatic rings of adjacent bipyridyl linker ligands, leading to a 3-D supramolecular network in the solid state (Figure 2(b)).

3.2.3. [Zn(N₃)₂(L)]ₙ (3)

In contrast to **1** and **2**, compound **3** crystallizes in the orthorhombic space group *Pbca*. As depicted in Figure 3(a), the zinc cation adopts distorted tetrahedral geometry with τ_4 index of 0.87. The cation is coordinated to two nitrogen atoms of two azido co-ligands and two nitrogen atoms of two L linkers. Terminal coordination of the azido

co-ligands leads to the formation of $[Zn(N_3)_2]$ nodes; they are linked by L ligands to a 1-D coordination polymer. The steric hindrance of the azido ligands reduces the N1A–Zn1–N1X angle to 100° and results in a zigzag chain parallel to the [0 0 1] direction. Literature reports confirm that tetrahedral coordination is abundant for zinc complexes [47–49]. Several compounds comprising a zinc(II) center, 4,4′-bipyridine analogue ligands and azido ancillary ligands have been described, for example the 3-D structure $[Zn(TPB)(N_3)_2]_n$ (TPB = 1,2,3,4-*tetra*-(4-pyridyl)-butane) [50], which exhibits octahedral coordination geometry and azido ligands both in end-to-end and terminal coordination.

π–π Stacking with closest C···C distances of 3.31 and 3.38 Å between the bipyridine groups of adjacent chains represents the shortest and presumably most relevant interchain contact stabilizing the 3-D network (Figure 3(b)).

3.3. Thermal stability

The thermal properties of Zn(II) coordination polymers **1–3** were investigated by thermogravimetric analysis (TGA) and single differential thermal analysis (SDTA) from 25–800 °C. The result for **1** is depicted in Supporting Information Figure S11: a small nonstoichiometric amount of surface-attached ethanol evaporates between 50 and 150 °C. The polycrystalline sample is thermally stable up to 180 °C, after which degradation occurs in two steps. The first weight loss between 180 and 360 °C is probably due to decomposition of L and one part of the acetate co-ligands (found 32.04%, Calcd 32.50%). The second step at 360–520 °C can be attributed to elimination of the remaining acetate groups (found 29.80%, Calcd 29.32%). The residual mass at $T > 530$ °C mostly represents ZnO (found 33.62%, Calcd 31.88%) in good crystallinity (Supporting Information Figure S12). The SDTA curve displays two exothermic peaks at 290 and 465 °C. Compound **2** exhibits the highest thermal stability (Supporting Information Figure S13). It starts to decompose at 240 °C with the loss of the central spacer fragment of the N,N′-donor ligand (found 24.76%, Calcd 24.41%). Between 460 and 650 °C the remaining fragments of the organic ligand and the anionic co-ligands are completely removed (found 57.83%, Calcd 56.31%). The remnant solid is mainly comprised of ZnO (found 17.30%, Calcd 16.85%), albeit with very low crystallinity (Supporting Information Figure S14). The SDTA pattern exhibits two exothermic events at 315 and 555 °C. Compound **3** (Supporting Information Figure S15) starts to decompose at 160 °C, corresponding to loss of the naphthalene fragment from the N,N′-donor (found 30.65%, Calcd 31.60%). The second stage of decomposition takes place from 335 to 565 °C, in which removal of the remnant organic ligand and azide co-ligands are observed (found 52.07%, Calcd 52.32%). The solid remaining at 570 °C can be attributed to moderately crystalline (Supporting Information Figure S16) ZnO (found 16.92%, Calcd 16.75%). As shown in Supporting Information Figure S15 two exothermic peaks at 315 and 510 °C appear in the SDTA curve. To summarize, in **1–3** the presence of different anionic co-ligands and variations in coordination geometry of the metal centers affects the structural properties and leads to differences in thermal stability and decomposition pathways. The final decomposition product is ZnO in

Table 2. Calculated NBO charges, electron distribution, Wiberg bond index, and second-order perturbation energies in **2**.

Atom	Net charge	Electron configuration	Donor	Acceptor	WBI	$E2$ (kcal mol^{-1})	$D(M - X)$ Å
Zn1	1.29212	[core]4S(0.30)3d(9.98)4p(0.43)					
O1	−0.75872	[core]2S(1.65)2p(5.09)	O1$_{LP}$	Zn1$_{LP*}$	0.2423	93.11	2.003(4)
O2	−0.78027	[core]2S(1.66)2p(5.11)	O2$_{LP}$	Zn1$_{LP*}$	0.2499	94.6	1.981(4)
N1	−0.73522	[core]2S(1.45)2p(4.26)3S(0.01)3p (0.01)3d(0.01)	N1$_{LP}$	Zn1$_{LP*}$	0.3314	104.85	1.967(5)
N2	−0.52592	[core]2S(1.35)2p(4.16)3p(0.01)	N2$_{LP}$	Zn1$_{LP*}$	0.1686	52.34	2.173(4)
N5	−0.51578	[core]2S(1.34)2p(4.16)3p(0.01)	N5$_{LP}$	Zn1$_{LP*}$	0.1616	49.84	2.215(4)

all cases, but this solid is obtained in different degrees of crystallinity as evidence by the powder patterns.

### 3.4. Natural bond orbital (NBO) analysis

NBO analysis is an effective tool to provide detailed insight into the electronic properties of compounds such as electron configuration, atomic charges and Wiberg bond index (WBI). The electron configuration analysis compiled in Table 2, Supporting Information Tables S4 and S5 shows that the Zn(II) ions interact with the ligands mainly via 4s, 3d, and 4p orbitals. The O and N donor atoms coordinate via their lone pair electrons in the 2s and 2p orbitals. The distribution of electron density over the molecule can also strengthen the metal-ligand interactions. The natural charges on the metal ions are much lower than +2, thus implying a significant donation of electron density from the ligands to the central metal ions. A similar conclusion can be deduced from the Wiberg bond index (WBI) calculation, which expresses the bond order; the WBI values account for bonding interactions between the metal ion and donor atoms with a covalent contribution. The NBO WBI of the metal-ligand bonds are in good agreement with the experimentally determined crystal structure data, where a greater WBI corresponds to a shorter bond distance.

The natural bond orbital analysis provides a method for investigation of the intra- and intermolecular interactions based on the delocalization of electron density between occupied Lewis-type orbitals (Lewis-type NBOs) and formally unoccupied orbitals (non-Lewis NBOs). This delocalization is referred to as delocalization correction to the 0th-order natural Lewis structure. It corresponds to stabilization of a donor-acceptor interaction according to the stabilization energy E(2), which results from second-order perturbation theory. This delocalization effect is one of the influential factors on the coordination environment of the metal cation and may act as driving force in the self-assembly of coordination polymers. In **1**–**3**, the most relevant contributions result from n-n^* interactions between the lone-pairs of oxygen and nitrogen orbitals with the anti-lone-pair of the metal orbitals. A larger value for E(2) implies a more effective interaction between metal cations and coordinated atoms. As summarized in Table 2, Supporting Information Tables S4 and S5, there is an inverse correlation between E(2) and the metal-donor bond length determined by X-ray diffraction. Their relationship implies that larger stabilization energy is related to shorter bond distance.

LUMO

HOMO
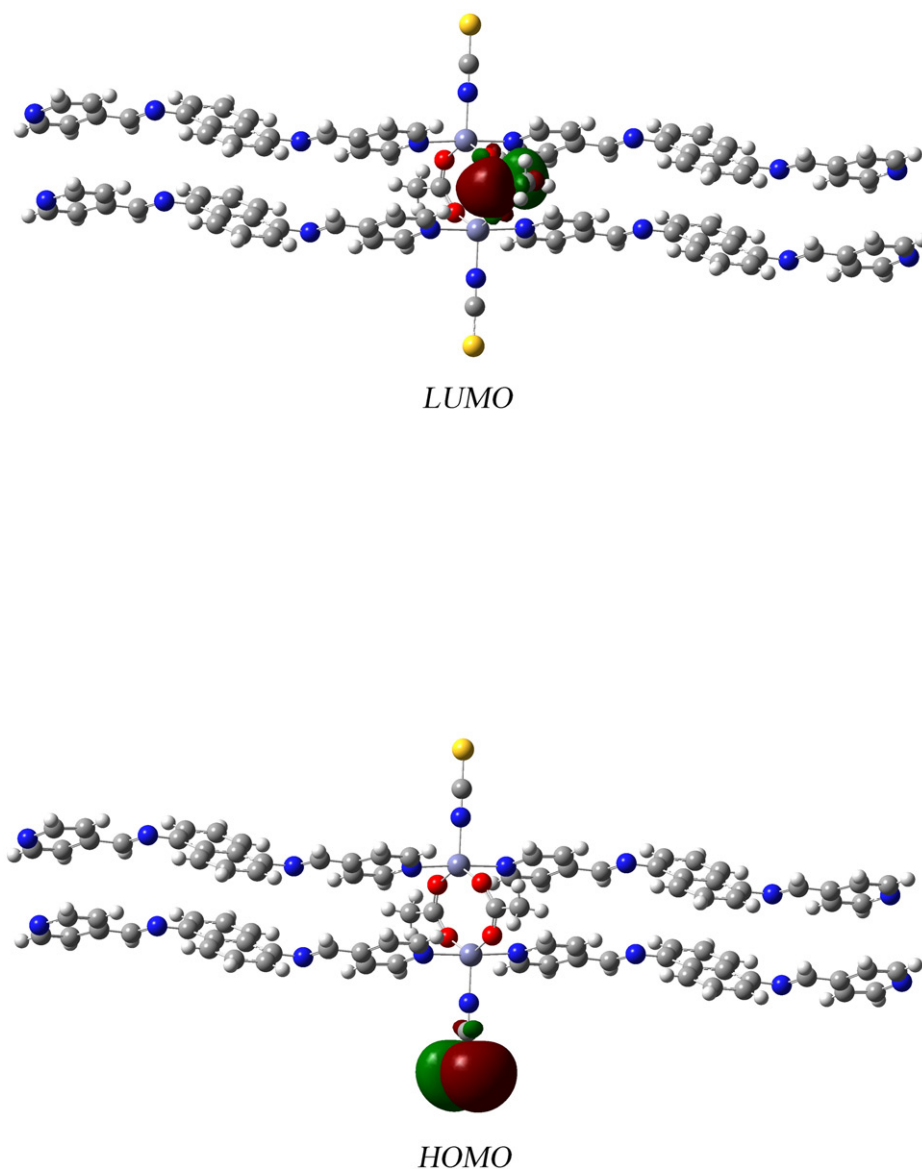
Figure 4. Graphical presentation of calculated frontier orbitals of [Zn(NCS)(OAc)(L)]$_n$ **2**.

Knowledge of the localization of frontier molecular orbitals is important in order to understand electronic and optical properties. Such analysis of frontier molecular orbitals can be used to evaluate chemical stability, the nature of reactivity and certain structural and physical properties of molecules and extended materials [51–53]. The 3-D plot shows that the highest occupied molecular orbital (HOMO) in **1** is essentially localized at the aromatic rings of the bipyridine ligand, whereas the lowest unoccupied molecular orbital (LUMO) is centered on the bridging acetato co-ligand (Supporting Information Figure S17). Thus, ligand-to-ligand charge transfer can be inferred from the shape of the molecular orbitals. As shown in Figure 4, the HOMO of **2** is mainly derived from the thiocyanato co-ligand and the LUMO from the bridging
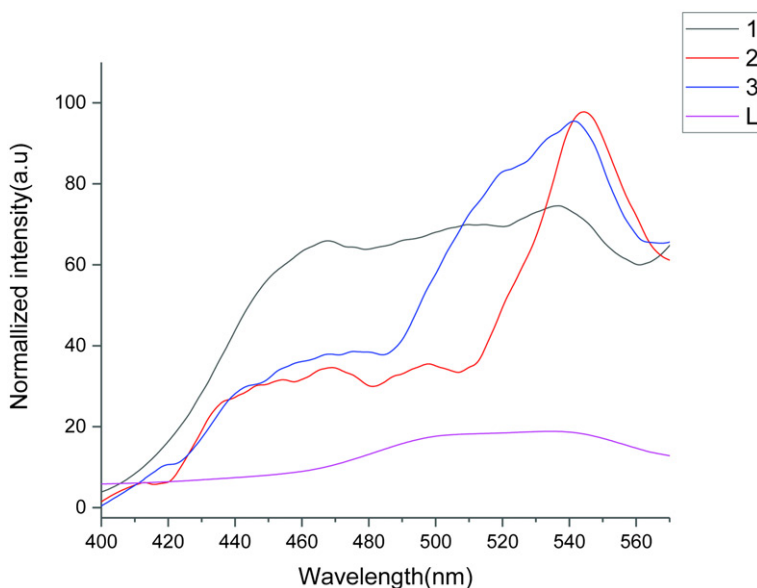
Figure 5. Solid-state emission spectra of L and **1**–**3** at room temperature.

acetato ligands, which implies that ligand-to-ligand transitions are expected. Both lowest unoccupied and highest occupied molecular orbital of **3** are localized on the naphthalene ring of the *N,N'*-donor ligand. Thus, intraligand charge transfer can be assumed (Supporting Information Figure S18).

3.5. UV–Vis and luminescence properties

The solid–state UV–Vis spectra for the uncoordinated ligand L and compounds **1**–**3** are shown in Supporting Information Figure S19. L is associated with two main absorption bands at 313 nm and 400 nm, arising from the π–π^* and n–π^* transitions in the aromatic system. The absorption bands of **1**–**3** do not vary strongly when compared to those of the free ligand, demonstrating that coordination hardly alters the intrinsic electronic properties of L. Moreover, the appearance of several absorption peaks or shoulders for the given chromophore is common for highly conjugated systems. This fine structure reflects electronic transitions between the different vibrational energy levels possible for each electronic state.

The luminescence properties of **1**–**3** and L were investigated in the solid state at room temperature (Figure 5). Free L exhibits a broad emission band at 520 nm upon excitation at 310 nm, which can be attributed to intraligand π–π^* emissions. **1** exhibits a broad emission band with a maximum at 536 nm (λ_{ex} = 310 nm), which spreads from blue to green wavelengths. As the maximum emission displays a slight red-shift in comparison to L, we assume that the luminescence is due to ligand-centered electronic transitions within the aromatic systems. Compound **2** shows an intense emission at 544 nm (λ_{ex} = 310 nm), red-shifted with respect to the free ligand emission, and an additional weaker broad emission band between 429 and 506 nm; the latter can probably be attributed to ligand-to-ligand charge transfer. Complex **3** shows two

maxima of luminescence at 538 nm and 454 nm. The band at 540 nm is comparable to that in the ligand and can be ascribed to intraligand charge transfer.

Luminescence is more intense for the complexes than for the uncoordinated ligand because metal coordination effectively increases the conformational rigidity of the ligands and hence decreases the nonradiative decay of intraligand excited states [54, 55].

4. Conclusion

This work presents the syntheses of three new 1-D coordination polymers, $[Zn_7(\mu_4\text{-}O)_2(OAc)_{10}(L)]_n$ (**1**), $[Zn(NCS)(OAc)(L)]_n$ (**2**), and $[Zn(N_3)_2(L)]_n$ (**3**), and their spectroscopic and structural characterization. Complexes **1**–**3** are based on the linker *N,N'-bis*(pyridin-4-ylmethylene)naphthalene-1,5-diamine. This ligand together with the variable coordination mode of the Zn(II) cations and different anionic co-ligands generates chain, ladder-like and zigzag 1-D polymer coordination. Beyond these motifs based on strong coordinative bonds, supramolecular interactions involving π–π stacking and nonclassical hydrogen bonds lead to stable 3-D networks. The intraligand N···N distance amounts to about 16 Å in all three compounds. L proves semi-rigid, with coplanar pyridyl rings for reasons of symmetry in **1** and very small dihedral angles of 2.9(3) and 4.5(3)° in **2** and **3**, respectively. The central naphthalene system and the peripheral pyridyl rings subtend interplanar angles of 57° in **1** and 34°–39° in **2** and **3**, thus making L an attractive component for crystal engineering with rather predictable geometry. The polymers differ with respect to thermal stability and decomposition modes, reflecting the effect of the anionic co-ligands and coordination geometry on the architecture of the extended structures. The fluorescence properties of **1**–**3** suggest their potential as hybrid organic–inorganic photoactive materials. NBO analysis shows the importance of ligand to cation charge transfer as driving force in the self-assembly process.

Disclosure statement

ORCID

Ulli Englert http://orcid.org/0000-0002-2623-0061

References

[1] D. Davarcı, R. Gür, S. Beşli, E. Şenkuytu, Y. Zorlu. *Acta Crystallogr. Sect. B*, **72**, 344 (2016).
[2] Z.-T. Zhang, Y.-Y. Wang, R. Yang, R. Liu, Y. Zhao, G.-H. Cui. *Transition Met. Chem.*, **41**, 169 (2016).
[3] B. Yotnoi, N. Meundaeng, W. Funfuenha, M. Pattarawarapan, T.J. Prior, A. Rujiwatra. *J. Coord. Chem.*, **68**, 4184 (2015).
[4] S.R. Batten, B. Chen, J.J. Vittal. *ChemPlusChem*, **81**, 669 (2016).
[5] K. Banerjee, S. Roy, M. Kotal, K. Biradha. *Cryst. Growth Des.*, **15**, 5604 (2015).

[6] Y. Cheng, M.-L. Yang, H.-M. Hu, B. Xu, X. Wang, G. Xue. *J. Solid State Chem.*, **239**, 121 (2016).

[7] L.F. Marques, M.V. Marinho, C.C. Correa, N.L. Speziali, R. Diniz, F.C. Machado. *Inorg. Chim. Acta*, **368**, 242 (2011).

[8] W. Kan, J.i. Yang, Y.Y. Liu, J.F. Ma. *CrystEngComm*, **14**, 6271 (2012).

[9] S. Millan, G. Makhloufi, C. Janiak. *Crystals*, **8**, 30 (2018).

[10] C.-Y. Su, A.M. Goforth, M.D. Smith, H.-C. Zur Loye. *Chem. Commun.*, **0**, 2158 (2004).

[11] D. Min, B.-Y. Cho, S.W. Lee. *Inorg. Chim. Acta*, **359**, 577 (2006).

[12] Y.O. Jang, S.W. Lee. *Polyhedron*, **29**, 2731 (2010).

[13] S.H. Kim, H.S. Huh, S.W. Lee. *J. Mol. Struct.*, **841**, 78 (2007).

[14] F. Li, J.K. Clegg, C.J. Kepert. *J. Inclusion Phenom. Macrocycl. Chem.*, **71**, 381 (2011).

[15] B. Shaabani, N. Rad-Yousefnia, M. Zahedi, Ş. Ertan, G.R. Blake, M.S. Zakerhamidi. *Inorg. Chim. Acta*, **455**, 158 (2017).

[16] M. Zahedi, B. Shaabani, U. Englert, N. Rad-Yousefnia, G.R. Blake, C. Kazak. *Polyhedron*, **133**, 110 (2017).

[17] M. Zahedi, B. Shaabani, M. Aygün, C. Kazak. *Inorg. Chim. Acta*, **469**, 461 (2018).

[18] K.-Y. Zou, Q. Zou, T. Han, Y.-C. Liu, J.-J. Wang, X. Zhang, Z.-X. Li. *J. Solid State Chem.*, **235**, 85 (2016).

[19] A. Beheshti, V. Nobakht, L. Carlucci, D.M. Proserpio, C. Abrahams. *J. Mol. Struct.*, **1037**, 236 (2013).

[20] J.L. Sague, M. Meuwly, K.M. Fromm. *CrystEngComm*, **10**, 1542 (2008).

[21] M. Zahedi, B. Shaabani, U. Englert, J. van Leusen. *Z. Kristallogr.*, **233**, 97 (2018).

[22] M. Du, Z.-H. Zhang, X.-G. Wang, L.-F. Tang, X.-J. Zhao. *CrystEngComm*, **10**, 1855 (2008).

[23] R. Bikas, H. Hosseini-Monfared, L. Sieroń, A. Gutiérrez. *J. Coord. Chem.*, **66**, 4023 (2013).

[24] P. Saint. *Data reduction software (Version 7.68 A)*, Bruker AXS Inc., Madison, WI (2009).

[25] G.M. Sheldrick. *SADABS (version 2.03). Program for empirical absorption correction of area detector data*, University of Göttingen, Göttingen, Germany (2004).

[26] *CrysAlisPro*. Agilent Technologies Ltd., Yarnton, Oxfordshire, UK (2013).

[27] G.M. Sheldrick. *Acta Crystallogr. Sect. A*, **64**, 112 (2008).

[28] G.M. Sheldrick. *Acta Crystallogr. C*, **71**, 3 (2015).

[29] A.L. Spek. *Acta Crystallogr. C*, **71**, 9 (2015).

[30] M. Frisch, G. Trucks, H. Schlegel, G. Scuseria, M. Robb, J. Cheeseman, J. Montgomery Jr., T. Vreven, K. Kudin, J. Burant. *Gaussian 03, Revision C.02*, Gaussian, Inc., Wallingford, CT (2004).

[31] P. Stephens, F. Devlin, C. Chabalowski, M.J. Frisch. *J. Phys. Chem.*, **98**, 11623 (1994).

[32] W.J. Hehre, R.F. Stewart, J.A. Pople. *J. Chem. Phys.*, **51**, 2657 (1969).

[33] A. Petersson, A. Bennett, T.G. Tensfeldt, M.A. Al-Laham, W.A. Shirley, J. Mantzaris. *J. Chem. Phys.*, **89**, 2193 (1988).

[34] H.-L. Hu, M.-C. Suen, C.-W. Yeh, J.-D. Chen. *Polyhedron*, **24**, 1497 (2005).

[35] G. Deacon, R. Phillips. *Coord. Chem. Rev.*, **33**, 227 (1980).

[36] C. Näther, S. Wöhlert, J. Boeckmann, M. Wriedt, I. Jeß. *Z. Anorg. Allg. Chem.*, **639**, 2696 (2013).

[37] K. Nakamoto. *Infrared and Raman spectra of Inorganic and Coordination Compounds*, 4th edn, Wiley, New York, NY (1986).

[38] A. Beheshti, A. Lalegani, G. Bruno, H.A. Rudbari. *J. Mol. Struct.*, **1071**, 18 (2014).

[39] L. Yang, D.R. Powell, R.P. Houser. *Dalton Trans.*, 955 (2007).

[40] M.T. Ng, T.C. Deivaraj, J.J. Vittal. *Inorg. Chim. Acta*, **348**, 173 (2003).

[41] J. Granifo, M.T. Garland, R. Baggio. *Polyhedron*, **25**, 2277 (2006).

[42] A. Waheed, R.A. Jones, J. McCarty, X. Yang. *Dalton Trans.*, 3840 (2004).

[43] A.W. Addison, T.N. Rao, J. Reedijk, J. van Rijn, G.C. Verschoor. *J. Chem. Soc. Dalton Trans.*, 1349 (1984).

[44] C.R. Groom, F.H. Allen. *Angew. Chem. Int. Ed. Engl.*, **53**, 662 (2014).

[45] S. Bhattacharya, U. Sanyal, S. Natarajan. *Cryst. Growth Des.*, **11**, 735 (2011).

[46] X. Li, R. Cao, D. Sun, W. Bi, Y. Wang, X. Li, M. Hong. *Cryst. Growth Des.*, **4**, 775 (2004).

[47] S. Yoshioka, Y. Inokuma, V. Duplan, R. Dubey, M. Fujita. *J. Am. Chem. Soc.*, **138**, 10140 (2016).

[48] P. Yang, M.-S. Wang, J.-J. Shen, M.-X. Li, Z.-X. Wang, M. Shao, X. He. *Dalton Trans.*, **43**, 1460 (2014).

[49] M.T. Ng, T.C. Deivaraj, W.T. Klooster, G.J. McIntyre, J.J. Vittal. *Chemistry*, **10**, 5853 (2004).

[50] J.-G. Lin, F.-M. Wang, Y.-Y. Xu, C.-S. Lu, Q.-J. Meng, P.-H. Wu. *Inorg. Chim. Acta*, **362**, 5219 (2009).

[51] P.K. Chattaraj. *J. Phys. Chem. A*, **105**, 511 (2001).

[52] S.W. Hunt, K.R. Leopold. *J. Phys. Chem. A*, **105**, 5498 (2001).

[53] K. Fukui. *Science*, **218**, 747 (1982).

[54] Z.Y. Fu, X.T. Wu, J.C. Dai, S.M. Hu, W.X. Du, H.H. Zhang, R.Q. Sun. *Eur. J. Inorg. Chem.*, **2002**, 2730 (2002).

[55] L.Y. Zhang, G.F. Liu, S.L. Zheng, B.H. Ye, X.M. Zhang, X.M. Chen. *Eur. J. Inorg. Chem.*, **2003**, 2965 (2003).